A Dual-Functional Sensing-Communication Waveform Design Based on OFDM

Yinghui He, *Member, IEEE*, Guanding Yu, *Senior Member, IEEE*,
Zhenzhou Tang, *Senior Member, IEEE*, Jianfeng Wang, and Haiyan Luo

***Abstract*—Integrated sensing and communication (ISAC) has emerged as a pivotal technology for next-generation mobile networks to embed sensing function on communication waveforms. A major challenge in ISAC is the effective integration of sensing and communication functions. Addressing this, this paper introduces a dual-functional waveform design that builds on the existing orthogonal frequency division multiplexing (OFDM) waveform. Unlike prior approaches that generally sacrifice communication performance to enhance sensing performance, our design contains a null-space sensing precoder that utilizes the null space of the communication channel to project additional sensing signals, thus improving the sensing functionality of the OFDM waveform without degrading any communication performance. We formulate a waveform optimization problem aimed at maximizing the sensing performance under the null-space sensing precoder and then propose a majorization-minimization (MM)-based waveform design algorithm. Additionally, to meet the real-time communication requirement in practice, we analyze the intrinsic characteristics of the high-performance sensing waveform and then develop a low-complexity waveform design algorithm. Simulation results show that the proposed MM-based algorithm can dramatically improve sensing performance without incurring any additional sensing power and degrading the communication performance. Furthermore, the low-complexity algorithm achieves substantial improvements in the sensing performance with much reduced computational complexity.**

***Index Terms*—Integrated sensing and communication, waveform design, OFDM waveform, majorization-minimization, precoding**

I. Introduction

Different from traditional communication that connects people and things, merely pursuing high-speed, low-latency, and high-reliability communication, the next-generation mobile networks aim to achieve the transformation to connected intelligence and establish a smart society [1]–[3]. Realizing this goal requires more than just the communication function provided by 5G networks, and thus the next-generation (6G) cellular system necessitates native intelligence, communication, and sensing functions [4]–[7]. As a response to this need, integrated sensing and communication (ISAC) has emerged, aiming at providing native sensing capability on the 6G communication [8]–[10]. It leverages the sensing capability of wireless radio frequency (RF) signals, which has been proven effective in various sensing applications such as positioning, tracking, gesture recognition, and imaging [11]–[14]. The key challenge for realizing ISAC is the efficient integration of two functions within a single hardware.

The most straightforward approach to integrate sensing and communication functions involves the orthogonal resource allocation across the temporal domain [15], [16], spectral domain [17], [18], or spatial domain [19]. However, this method is inefficient as it fails to explore the potential of wireless signals to communicate and sense simultaneously. Consequently, recent studies have investigated the possibility of reusing communication signals for sensing [20], [21]. In communication systems, pilot signals, known for their low autocorrelation sidelobes, are crucial for time synchronization and channel estimation. These features are also beneficial for sensing systems that aim at detecting echoes from surrounding targets. Thus, pilots in Wi-Fi and cellular systems have been extensively explored for sensing applications [22], [23]. However, pilots constitute a minor fraction of the resources, typically less than 0.1 % in Wi-Fi systems.[1] This small ratio limits their overall utility for comprehensive sensing tasks.

To enhance ISAC efficiency, leveraging data signals for sensing emerges as a preferable strategy. Unlike pilots, data signals occupy a larger proportion (almost 100%) of communication resources. Yet, this approach presents challenges. Sensing systems require signals with low autocorrelation, however, the random data signals are hard to satisfy the requirement. Therefore, directly using these data signals for sensing often results in poor performance. Meanwhile, modern communication systems predominantly utilize the orthogonal frequency division multiplexing (OFDM) technique to boost the communication performance. Therefore, our research focuses on enhancing the sensing performance of the OFDM data waveform, aiming to reconcile the conflicting requirements of high-quality communication and effective sensing within a single waveform.

Manuscript received April 27, 2024; revised July 10, 2024; accepted August 15, 2024. The work of Zhenzhou Tang was supported by the Natural Science Foundation of Zhejiang Province, China, under Grant LZ20F010008. (*Corresponding author: Z. Tang.*)

Y. He and G. Yu are with the College of Information Science and Electronic Engineering, Zhejiang University, Hangzhou 310027, China. e-mail: {2014hyh, yuguanding}@zju.edu.cn.

Z. Tang is with Wenzhou Key Laboratory for Intelligent Networking, Wenzhou University, Wenzhou 325035, China. e-mail: mr.tangzz@gmail.com.

J. Wang is with Lenovo Research, Lenovo Group Ltd., Beijing 100094, China. e-mail: wangjf20@lenovo.com.

H. Luo is with Lenovo (Shanghai) Information Technology Co., Ltd, Shanghai 201203, China. e-mail: luohy7@lenovo.com.

[1]In the IEEE 802.11a standard [24], pilots in a packet, including short training field (STF) and long training field (LTF), only have a duration of 16 us. Meanwhile, the MAC frame has a maximum length of 2,348 bytes, corresponding to a duration of 30 ms with the data rate being 6 Mbps. Thus, we can obtain the occupancy ratio of pilots as nearly 0.05 %.

A. Related Works

The waveform design for achieving ISAC mainly includes three kinds of methods: sensing-centric design scheme [25]–[31], communication-centric design scheme [32], [33], and joint design scheme [34]. The sensing-centric design scheme embeds communication symbols within existing sensing waveforms and prioritizes sensing performance. There are two mainstream approaches. The first is based on the chirp waveforms, where the main strategy involves modulating communication symbols onto the chirp through intrapulse or interpulse modulation techniques [25], [26]. For example, [26] proposed to modulate communication symbols onto the chirp's modulation frequency. Although this direct design does not affect sensing performance, the efficiency of information delivery is extremely low. To improve the communication rate, a feasible approach is embedding a series of communication symbols into each chirp or orthogonal waveform [27]–[29]. For instance, [28] proposed to modulate communication symbols as the phase variation over the fast time into a linear frequency modulation (LFM) sensing waveform. The second approach is the index modulation technique. When M orthogonal waveforms are transmitted via M antennas, information delivery can be achieved by scrambling the sequence of waveforms on different antennas [30], [31]. Theoretically, this technique can carry $\log_2 M!$ bits per transmission.

The communication-centric design scheme aims to modify existing communication waveforms to achieve higher sensing performance. [32] proposed a sparse signal coding method and the corresponding codebook for communication data, and theoretically proved that the proposed method could reduce the autocorrelation sidelobes of the transmit signal. Differently, [33] optimized each symbol in the transmit signal directly and developed an algorithm based on the majorization-minimization (MM) method to suppress the autocorrelation sidelobes, while keeping the symbol deviation within a certain range.

On the other hand, the joint design scheme is realized through optimization. [34] optimized the communication signal, aiming to minimize the distance between the received signal at the receiver and the original communication signal on one hand, and to minimize the distance between the transmit signal and a known high-performance sensing waveform on the other hand. An algorithm to balance between sensing and communication performance was proposed. Although the above designs can effectively enhance sensing performance, they also lead to a decrease in communication performance, e.g., bit error rate and communication rate.

B. Main Contributions

Unlike existing approaches that generally improve sensing performance by sacrificing communication performance, we aim to improve the sensing performance of the OFDM data waveform without degrading communication performance. Meanwhile, we note that the cyclic prefix (CP), adopted in OFDM systems to avoid inter-symbol interference (ISI), introduces a null space of the channel between the transmitter and receiver. This null space, previously leveraged for the coexistence of dual communication systems [35], [36], now serves a novel purpose in our study. In particular, we propose a null-space sensing precoder that utilizes the null space to enhance sensing capability by projecting additional sensing signals into it. Different from the existing work [33] that improves sensing performance by sacrificing communication performance, our proposed method can improve sensing performance without impacting communication performance. To optimize these additional sensing signals for superior sensing performance, we formulate a waveform design problem centered on minimizing the autocorrelation sidelobes of the transmit signal. To solve the problem, we propose a waveform design algorithm based on the MM method. Additionally, we develop a low-complexity algorithm to meet the real-time communication requirement in practical systems.

The main contributions of this work are summarized as follows.

- We propose a novel dual-functional waveform design method that contains a special null-space sensing precoder. The precoder utilizes the null space of the communication channel to improve the sensing performance by projecting extra sensing signals into the null space. It does not affect the received data signals at the communication receiver, thus preserving the original communication performance.
- We formulate a waveform optimization problem to maximize the sensing performance. To solve it, we propose an MM-based waveform design algorithm where the closed-form solution is derived in each iteration. We prove that the proposed algorithm can be guaranteed to converge to a stationary point of the original problem.
- Considering the real-time communication demand in some scenarios, we analyze the intrinsic characteristics of the waveform with high sensing performance and then develop a low-complexity algorithm without iteration. Numerical results illustrate performance gains achieved by the proposed waveform design algorithms over the conventional OFDM waveform.

C. Organization

The rest of this paper is organized as follows. Section II introduces the system model and formulates the optimization problem. In Section III, we develop an MM-based algorithm to solve the problem. A low-complexity algorithm is developed in Section IV. Simulation results are presented in Section V, and the whole paper is concluded in Section VI.

Notations: In this paper, scalars are denoted by lower case, vectors are denoted by boldface lower case, and matrices are denoted by boldface upper case. $\boldsymbol{I}$ represents an identity matrix and $\mathbf{0}$ denotes an all-zero vector. $(\cdot)^*$, $(\cdot)^T$, and $(\cdot)^H$ denote complex conjugate, transpose, and Hermitian transpose, respectively. For a matrix $\boldsymbol{A}$, vec$(\boldsymbol{A})$ represents the operation of vectorization that linearly converts the matrix into a vector, tr$(\boldsymbol{A})$ is the trace of $\boldsymbol{A}$, and $||\boldsymbol{A}||$ denotes the Frobenius norm of $\boldsymbol{A}$. For a vector $\boldsymbol{a}$, Diag$(\boldsymbol{a})$ denotes a diagonal matrix with each diagonal element being the corresponding element in $\boldsymbol{a}$, and $||\boldsymbol{a}||$ represents its Euclidean norm. $\mathcal{R}\{\cdot\}$ ($\mathcal{I}\{\cdot\}$)

denotes the real (imaginary) value of a complex scalar and $|\cdot|$ represents the absolute value of a complex scalar. $\mathbb{C}^{m\times n}$ ($\mathbb{R}^{m\times n}$) denotes the space of $m \times n$ complex (real) matrix.

II. System Model and Problem Statement

In this section, we introduce the ISAC system model and the dual-functional signal model. Then, we propose a novel waveform design method and mathematically formulate the optimization problem of interest.

A. System Model

As shown in Fig. 1, we consider a broadband ISAC system, consisting of one single-antenna BS and one single-antenna user.[2] The BS aims to transmit a dual-functional signal for sending communication data to the user and detecting the echo signals from surrounding potential targets, simultaneously.[3] The communication process can be divided into two parts, i.e., pilot transmission and data transmission, and we focus on the latter since it occupies the major part of the total communication period. To adapt to existing communication systems, we assume that the user applies the OFDM technique to demodulate the received signals since OFDM has been widely adopted in the 4G, 5G, and Wi-Fi communication systems.

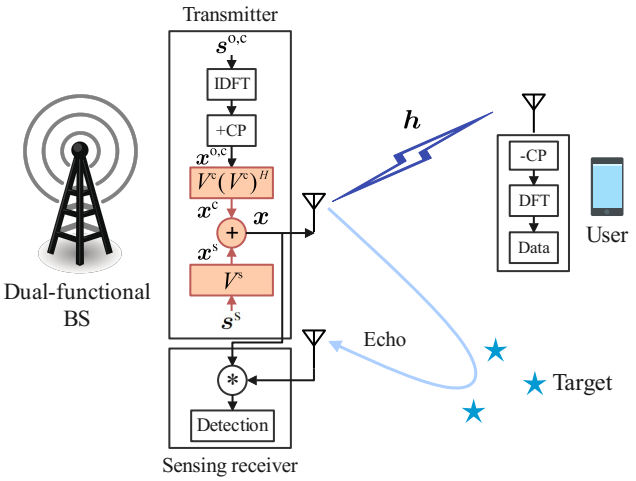

Fig. 1. An ISAC system model, where we propose to add some parts marked with a special color into the transmitter of the BS for improving the sensing performance of OFDM signals.

B. Dual-Functional Signal Model

Due to the frequency selective fading caused by the multipath effect, severe ISI will be incurred by the direct transmission. To avoid it, the OFDM technique is adopted and the data is transmitted parallelly over different subcarriers by using the inverse discrete Fourier transform (IDFT) operation and inserting a CP. Let $\boldsymbol{s}^{\mathrm{o,c}} \in \mathbb{C}^{N\times 1}$ denote the data transmitted to the user with N being the number of subcarriers, and then the transmitted OFDM signals at the BS can be expressed as

$$\boldsymbol{x}^{\mathrm{o,c}} = \boldsymbol{A}\boldsymbol{F}^H \boldsymbol{s}^{\mathrm{o,c}}, \tag{1}$$

where $\boldsymbol{F} \in \mathbb{C}^{N\times N}$ denotes the discrete Fourier transform (DFT) matrix with the element at the k-th row and the l-th column being $e^{-i2\pi\frac{kl}{N}}/\sqrt{N}$ and $\boldsymbol{A} \in \mathbb{C}^{(N+L)\times N}$ represents the CP insertion matrix. Specifically, $\boldsymbol{A} \in \mathbb{C}^{(N+L)\times N}$ is used for appending the last L entries of its input vector to the beginning of itself, as

$$\boldsymbol{A} = \begin{bmatrix} \boldsymbol{0} & \boldsymbol{I}_L \\ & \boldsymbol{I}_N \end{bmatrix}. \tag{2}$$

Then, after undergoing the wireless channel between the BS and the user, denoted by $\boldsymbol{h} = [h_0, h_1, \cdots, h_L]^T$, and the operations of CP removal and DFT, the received signal at the communication user is

$$\begin{aligned} \boldsymbol{y}^{\mathrm{o,c}} &= \boldsymbol{F}\mathcal{T}(\boldsymbol{h})\boldsymbol{x}^{\mathrm{o,c}} + \boldsymbol{n} \\ &= \boldsymbol{F}\mathcal{T}(\boldsymbol{h})\boldsymbol{A}\boldsymbol{F}^H \boldsymbol{s}^{\mathrm{o,c}} + \boldsymbol{n}, \end{aligned} \tag{3}$$

where $\boldsymbol{n} \sim \mathcal{CN}(\boldsymbol{0}, \sigma^2\boldsymbol{I})$ is the complex circular Gaussian noise vector with zero mean and covariance $\sigma^2\boldsymbol{I}$ and $\mathcal{T}(\cdot)$ is Toeplitz operation that returns a Toeplitz matrix built from a given vector. Thus, the channel matrix $\mathcal{T}(\boldsymbol{h})$ can be expressed as

$$\mathcal{T}(\boldsymbol{h}) = \begin{bmatrix} h_L & \cdots & h_0 & 0 & \cdots & 0 \\ 0 & \ddots & & \ddots & \ddots & \vdots \\ \vdots & \ddots & \ddots & & \ddots & 0 \\ 0 & \cdots & 0 & h_L & \cdots & h_0 \end{bmatrix} \in \mathbb{C}^{N\times(N+L)}. \tag{4}$$

Thanks to the introduction of DFT and CP, the equivalent channel matrix $\boldsymbol{F}\mathcal{T}(\boldsymbol{h})\boldsymbol{A}\boldsymbol{F}^H$ is diagonal such that the data is parallelly transmitted over different subcarriers, and thus the ISI is avoided. However, the OFDM technique is designed purely for the communication purpose without considering the sensing performance.

Different from communication systems, sensing systems aim to detect the echo of the transmit signal from the target. Specifically, the received signal is first processed with a matched filter, that is, filtering the received signal using the complex conjugate of the transmit signal. Then, applying constant false alarm rate (CFAR) detection [40] on the filtered signal, the sensing system can determine whether the echo signal from a target is received by comparing the filtered signal with a pre-set threshold. When there are multiple targets, the filtered signal is the summation of the autocorrelation of the transmit signal with different time offsets and amplitude. Therefore, the autocorrelation from different targets may interfere with each other.

Fig. 2 plots the filtered signal when the conventional OFDM communication signal is directly used as the transmit signal and there are two targets, a weak one and a strong one. In Fig. 2(a), the filtered signals of two targets are separated, while

[2]The proposed waveform design in this paper can be easily extended to the multi-user scenario with the orthogonal frequency division multiple access (OFDMA) method and the time division multiple access (TDMA) method. Specifically, with the OFDMA method, a multi-user scenario is equivalent to the signal-user scenario studied in this paper by using the equivalent channel between the BS and users introduced in [37].

[3]In this paper, we focus on detecting the echo signal from the sensing target, a fundamental process in almost all sensing applications, such as localization and recognition [38], [39]. The detected echo can be separated from the received signal for subsequent sensing applications using existing sensing algorithms.

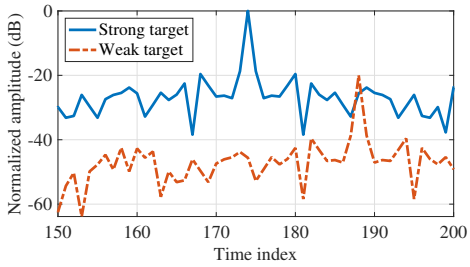

(a) Separated signals for two targets.

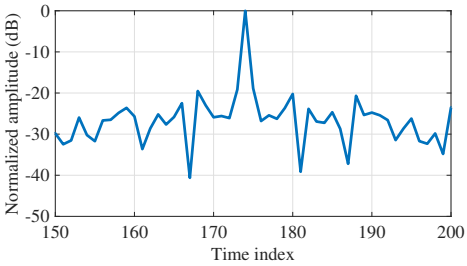

(b) Real filtered signal, i.e., the summation of two separated signals.

Fig. 2. Normalized filtered signals.

Fig. 2(b) shows the real filtered signal at the receiver which is the summation of two separated signals. It can be observed that the filtered signal's sidelobe of the strong target completely masks the filtered signal's peak of the weak target, making the weak target difficult to be detected. Thus, to improve the sensing performance, i.e., detection probability, we opt to reduce the sidelobe level of the autocorrelation for the transmit signal in this paper.

With the consideration that the proposed waveform should be as compatible as possible with existing communication systems, we aim to improve the sensing performance of the OFDM waveform while keeping the structure unchanged. To this end, the most direct method is to add an additional sensing signal, denoted by $\boldsymbol{x}^{\mathrm{o,s}}$, to the OFDM signal $\boldsymbol{x}^{\mathrm{o,c}}$, and the dual-functional signal can be expressed as

$$\boldsymbol{x} = \boldsymbol{x}^{\mathrm{o,c}} + \boldsymbol{x}^{\mathrm{o,s}}. \tag{5}$$

Then, the received signal at the communication user is

$$\boldsymbol{y} = \boldsymbol{F}\mathcal{T}(\boldsymbol{h})(\boldsymbol{x}^{\mathrm{o,c}} + \boldsymbol{x}^{\mathrm{o,s}}) + \boldsymbol{n}. \tag{6}$$

To reduce the impact caused by introducing an additional sensing signal $\boldsymbol{x}^{\mathrm{o,s}}$, the received signal at the user should not be impacted by $\boldsymbol{x}^{\mathrm{o,s}}$, i.e., $\boldsymbol{y} = \boldsymbol{y}^{\mathrm{o,c}}$. Thus, we propose a novel dual-functional waveform design method as shown in the following theorem.

Theorem 1. *The singular value decomposition (SVD) of $\mathcal{T}(\boldsymbol{h})$ is $\mathcal{T}(\boldsymbol{h}) = \boldsymbol{U}\boldsymbol{\Lambda}\boldsymbol{V}^H$ and $\boldsymbol{V} = [\boldsymbol{v}_1, \cdots, \boldsymbol{v}_{N+L}] \in \mathbb{C}^{(N+L)\times(N+L)}$ is an unity matrix with $\boldsymbol{v}_n$ being the n-th column vector. Then, to realize $\boldsymbol{y} = \boldsymbol{y}^{\mathrm{o,c}}$, the sensing signal should satisfy $\boldsymbol{x}^{\mathrm{o,s}} = \boldsymbol{V}^{\mathrm{s}}\boldsymbol{s}^{\mathrm{o,s}}$ where $\boldsymbol{V}^{\mathrm{s}} = [\boldsymbol{v}_{N+1}, \cdots, \boldsymbol{v}_{N+L}] \in \mathbb{C}^{(N+L)\times L}$ is the null-space sensing precoder, i.e., the null space of the wireless channel, and $\boldsymbol{s}^{\mathrm{s}} \in \mathbb{C}^{L\times 1}$ is the sensing symbol.*

Proof: The above statement can be easily proved since the size of $\mathcal{T}(\boldsymbol{h})$ is $N \times (N+L)$, the last L rows of $\boldsymbol{\Lambda}$ are all zeros and $\mathcal{T}(\boldsymbol{h})\boldsymbol{V}^{\mathrm{s}}$ is a zero matrix. ■

Based on Theorem 1, we propose a null-space sensing precoder $\boldsymbol{V}^{\mathrm{s}}$.[4] Using it, the sensing performance can be improved by optimizing the sensing signal without impacting the communication performance. Note that the time synchronization using the CP would not be influenced since we only modify the data waveform, and the time synchronization is realized using pilots. Moreover, the ISI can still be avoided since the received signal at the communication user is not affected. The autocorrelation of the transmit signal $\boldsymbol{x}$ can be expressed by

$$\begin{aligned} r_n &= \begin{cases} \sum_{i=0}^{N+L-n} x[i]^* x[i+n], & n = 0, 1, \cdots, N+L-1, \\ \sum_{i=0}^{N+L+n} x[i-n]^* x[i], & n = -N-L+1, \cdots, 0, \end{cases} \\ &= \boldsymbol{x}^H \boldsymbol{U}_n \boldsymbol{x}, \ \forall n \in \{-N-L+1, \cdots, N+L-1\}, \end{aligned} \tag{7}$$

where $\boldsymbol{U}_n$ is the matrix that the n-th sub-diagonal is 1 and all other elements are 0 and $x[i]$ is the n-th element of $\boldsymbol{x}$.

C. Transmit Power

Compared to the original OFDM communication signal $\boldsymbol{x}^{\mathrm{o,c}}$, a sensing signal $\boldsymbol{x}^{\mathrm{o,s}}$ is added into the transmit signal $\boldsymbol{x}$. The transmit power is not the summation of that of $\boldsymbol{x}^{\mathrm{o,c}}$ and $\boldsymbol{x}^{\mathrm{o,s}}$ since $\boldsymbol{x}^{\mathrm{o,c}}$ is not orthogonal to $\boldsymbol{x}^{\mathrm{o,s}}$. To calculate the transmit power, we can decompose the communication signal $\boldsymbol{x}^{\mathrm{o,c}}$ into two parts, i.e., $\boldsymbol{V}^{\mathrm{c}}(\boldsymbol{V}^{\mathrm{c}})^H\boldsymbol{x}^{\mathrm{o,c}}$ and $\boldsymbol{V}^{\mathrm{s}}(\boldsymbol{V}^{\mathrm{s}})^H\boldsymbol{x}^{\mathrm{o,c}}$, where $\boldsymbol{V}^{\mathrm{c}} = [\boldsymbol{v}_1, \boldsymbol{v}_2, \cdots, \boldsymbol{v}_N] \in \mathbb{C}^{(N+L)\times N}$ and $(\boldsymbol{V}^{\mathrm{s}})^H\boldsymbol{V}^{\mathrm{c}} = \boldsymbol{0}$. Therefore, the transmit power variation caused by adding $\boldsymbol{V}^{\mathrm{s}}\boldsymbol{s}^{\mathrm{o,s}}$ is

$$\Delta P = \frac{1}{N+L}\left(||\boldsymbol{s}^{\mathrm{o,s}} + (\boldsymbol{V}^{\mathrm{s}})^H\boldsymbol{x}^{\mathrm{o,c}}||^2 - ||(\boldsymbol{V}^{\mathrm{s}})^H\boldsymbol{x}^{\mathrm{o,c}}||^2\right). \tag{8}$$

To simplify the expression, we define $\boldsymbol{s}^{\mathrm{s}}$ as $\boldsymbol{s}^{\mathrm{o,s}} + (\boldsymbol{V}^{\mathrm{s}})^H\boldsymbol{x}^{\mathrm{o,c}}$ with $\boldsymbol{x}^{\mathrm{s}} = \boldsymbol{V}^{\mathrm{s}}\boldsymbol{s}^{\mathrm{s}}$ and define $\boldsymbol{x}^{\mathrm{c}}$ as $\boldsymbol{V}^{\mathrm{c}}(\boldsymbol{V}^{\mathrm{c}})^H\boldsymbol{x}^{\mathrm{o,c}}$. Then, the transmit signal can be rewritten as

$$\boldsymbol{x} = \boldsymbol{x}^{\mathrm{c}} + \boldsymbol{x}^{\mathrm{s}}. \tag{9}$$

The corresponding total transmit power is

$$P = P^{\mathrm{c}} + \Delta P = \frac{1}{N+L}\left(||\boldsymbol{x}^{\mathrm{c}}||^2 + ||\boldsymbol{s}^{\mathrm{s}}||^2\right), \tag{10}$$

where P^{c} represents the transmit power of the original OFDM communication signal $\boldsymbol{x}^{\mathrm{o,c}}$, as

$$\begin{aligned} P^{\mathrm{c}} &= \frac{1}{N+L}||\boldsymbol{x}^{\mathrm{o,c}}||^2 \\ &= \frac{1}{N+L}\left(||\boldsymbol{x}^{\mathrm{c}}||^2 + ||(\boldsymbol{V}^{\mathrm{s}})^H\boldsymbol{x}^{\mathrm{o,c}}||^2\right). \end{aligned} \tag{11}$$

D. Problem Formulation

In this paper, we aim to improve the sensing performance of the OFDM signal without compromising the communication

[4]Although we propose a null-space sensing precoder for the CP-OFDM waveform, the proposed method can also be applied to other CP-based waveforms (e.g., DFT-S-OFDM waveform) since it leverages the null space introduced by the CP.

performance under the transmit power limitation. To avoid the impact on communication performance, the sensing signal should satisfy the requirement in Theorem 1, i.e., $\boldsymbol{x}^{\mathrm{s}} = \boldsymbol{V}^{\mathrm{s}}\boldsymbol{s}^{\mathrm{s}}$. Meanwhile, the upper limit of the transmit power is denoted by $P^{\max}$. To improve the SNR of the echo, the transmit power should equal to its upper limit, i.e., $P = P^{\max}$. For the sensing performance, we focus on reducing the sidelobe level of the autocorrelation, that is, minimizing the ratio of the sidelobe level to the peak, as

$$\min \quad \frac{\sum_{n=-L}^{L} |r_n|^2 - |r_0|^2}{|r_0|^2}. \tag{12}$$

In the above, we mainly consider the sidelobe ranging from $-L$ to L since L represents the maximum coverage of the BS[5]. Moreover, we have

$$|r_0|^2 = |\boldsymbol{x}^H\boldsymbol{x}|^2 = ((N+L)P^{\max})^2. \tag{13}$$

Thus, $|r_0|^2$ is a constant and the objective function can be simplified as $\sum_{n=-L}^{L}|r_n|^2$. Combined with the above analysis, we formulate the waveform design problem to maximize the sensing performance, as

$$\begin{aligned}
\min_{\{\boldsymbol{x}^{\mathrm{s}},\boldsymbol{s}^{\mathrm{s}}\}} \quad & \sum_{n=-L}^{L} |r_n|^2 \\
& = \sum_{n=-L}^{L} \left|(\boldsymbol{x}^{\mathrm{c}}+\boldsymbol{x}^{\mathrm{s}})^H \boldsymbol{U}_n (\boldsymbol{x}^{\mathrm{c}}+\boldsymbol{x}^{\mathrm{s}})\right|^2, && \text{(14a)} \\
\text{s.t.} \quad & \boldsymbol{x}^{\mathrm{s}} = \boldsymbol{V}^{\mathrm{s}}\boldsymbol{s}^{\mathrm{s}}, && \text{(14b)} \\
& P = \frac{1}{N+L}\left(||\boldsymbol{x}^{\mathrm{c}}||^2 + ||\boldsymbol{s}^{\mathrm{s}}||^2\right) = P^{\max}. && \text{(14c)}
\end{aligned}$$

Existing works have proved that the objective function is non-convex and the constraint (14c) is also non-convex [41]. Solving Problem (14) directly is challenging due to the complex and nonconvex objective function, which has a computational complexity of $\mathcal{O}\left(N(N+L)\right)$. To address this, we propose a waveform design algorithm utilizing the MM method [42] in the following section. The main idea of the MM method is to simplify the objective function and reduce the computational complexity in each iteration.

III. Dual-Functional Waveform Design

In this section, we first introduce a brief overview of the MM method and then propose an MM-based waveform design algorithm to solve Problem (14).

A. MM Method

We briefly introduce the general framework of the MM method in the following. Consider the following problem

$$\begin{aligned}
\mathcal{P}: \quad \min_{\boldsymbol{z}} \quad & f(\boldsymbol{z}), && \text{(15a)} \\
\text{s.t.} \quad & \boldsymbol{z} \in \mathcal{Z}, && \text{(15b)}
\end{aligned}$$

where $f(\boldsymbol{z})$ is a differentiable function and $\mathcal{Z}$ is the feasible region. Instead of solving the above problem directly, the MM method seeks to sequentially solve a series of simple problems. Specifically, the update method in the l-th iteration is

$$\boldsymbol{z}^{(l+1)} = \operatorname{argmin}_{\boldsymbol{z}\in\mathcal{Z}} \bar{f}\left(\boldsymbol{z}; \boldsymbol{z}^{(l)}\right), \tag{16}$$

where $\bar{f}\left(\boldsymbol{z}; \boldsymbol{z}^{(l)}\right)$ is the surrogate function simplified from $f(\boldsymbol{z})$ at the point $\boldsymbol{z}^{(l)}$. Moreover, $\bar{f}\left(\boldsymbol{z}; \boldsymbol{z}^{(l)}\right)$ satisfies the following two requirements:

- $\bar{f}\left(\boldsymbol{z}; \boldsymbol{z}^{(l)}\right) \geq f(\boldsymbol{z}), \forall \boldsymbol{z} \in \mathcal{Z}$;
- $\bar{f}\left(\boldsymbol{z}^{(l)}; \boldsymbol{z}^{(l)}\right) = f(\boldsymbol{z}^{(l)})$.

These two requirements indicate that $\bar{f}\left(\boldsymbol{z}; \boldsymbol{z}^{(l)}\right)$ should be a globally tight upper bound of $f(\boldsymbol{z})$ for any $\boldsymbol{z} \in \mathcal{Z}$. Thus, minimizing $\bar{f}\left(\boldsymbol{z}; \boldsymbol{z}^{(l)}\right)$ results in a decrease in the objective function $f(\boldsymbol{z})$, as

$$f(\boldsymbol{z}^{(l+1)}) \leq \bar{f}\left(\boldsymbol{z}^{(l+1)}; \boldsymbol{z}^{(l)}\right) = f(\boldsymbol{z}^{(l)}). \tag{17}$$

Moreover, $f(\boldsymbol{z})$ continuously decreases with the progress of iterations, guaranteeing the convergence of the algorithm [43]. Therefore, by carefully designing $\bar{f}\left(\boldsymbol{z}; \boldsymbol{z}^{(l)}\right)$, the computational complexity of each iteration can be greatly reduced.

B. Waveform Design

To apply the MM method, we need to find a surrogate objective function. We first introduce the following lemma.

Lemma 1 [44]. *Give two Hermitian matrices, $\boldsymbol{A} \in \mathbb{C}^{n\times n}$ and $\boldsymbol{B} \in \mathbb{C}^{n\times n}$, and they satisfy $\boldsymbol{A} \succeq \boldsymbol{B}$, that is, $\boldsymbol{A}-\boldsymbol{B}$ is positive semi-definite. For any $\boldsymbol{z} \in \mathbb{C}^{n\times 1}$, $\boldsymbol{z}^H\boldsymbol{A}\boldsymbol{z}$ can be substituted by a surrogate function $\boldsymbol{z}^H\boldsymbol{B}\boldsymbol{z} + 2\mathcal{R}\left\{\boldsymbol{z}^H(\boldsymbol{A}-\boldsymbol{B})\boldsymbol{z}^{(l)}\right\} + (\boldsymbol{z}^{(l)})^H(\boldsymbol{B}-\boldsymbol{A})\boldsymbol{z}^{(l)}$ at the l-th iteration.*

Based on the above lemma, let $f(\boldsymbol{x}^s)$ denote the objective function (14a), and we have

$$\begin{aligned}
f(\boldsymbol{x}^{\mathrm{s}}) \leq \boldsymbol{w}^H\boldsymbol{B}_1\boldsymbol{w} + 2\mathcal{R}\left\{\boldsymbol{w}^H(\boldsymbol{A}_1-\boldsymbol{B}_1)\boldsymbol{w}^{(l)}\right\} \\
+ (\boldsymbol{w}^{(l)})^H(\boldsymbol{B}_1-\boldsymbol{A}_1)\boldsymbol{w}^{(l)}.
\end{aligned} \tag{18}$$

where $\boldsymbol{A}_1 \triangleq \sum_{n=-L}^{L} \operatorname{vec}\{\boldsymbol{U}_n\}\operatorname{vec}\{\boldsymbol{U}_n\}^H$ and $\boldsymbol{B}_1$ satisfies $\boldsymbol{B}_1 \succeq \boldsymbol{A}_1$. The details for deriving (18) can be found in Appendix A. Note that $\boldsymbol{B}_1$ could be $\lambda_1^{\max}\boldsymbol{I}$ with $\lambda_1^{\max}$ being the maximum eigenvalue of $\boldsymbol{A}_1$. Meanwhile, through simple mathematical analysis, $\operatorname{vec}\{\boldsymbol{U}_n\}/\sqrt{N+L-|n|}$, $n \in \{-L, \cdots, L\}$ is the eigenvector of $\boldsymbol{A}_1$ and the corresponding eigenvalue is $(N+L-|n|)$. Consequently, we can find that $\lambda_1^{\max} = N+L$. Furthermore, $\boldsymbol{w}^H\boldsymbol{B}_1\boldsymbol{w}$ in (18) can be further simplified as a constant, as

$$\boldsymbol{w}^H\boldsymbol{B}_1\boldsymbol{w} = (N+L)^3(P^{\max})^2. \tag{19}$$

Following the same way, we can find that $(\boldsymbol{w}^{(l)})^H(\boldsymbol{B}_1 - \boldsymbol{A}_1)\boldsymbol{w}^{(l)}$ is also a constant. Let C_1 denote the summation of the two constants. Then, (18) can be rewritten as

$$f(\boldsymbol{x}^{\mathrm{s}}) \leq 2\mathcal{R}\left\{\boldsymbol{w}^H(\boldsymbol{A}_1-\boldsymbol{B}_1)\boldsymbol{w}^{(l)}\right\} + C_1. \tag{20}$$

Since the surrogate function in the above is still directly related to $\boldsymbol{w}$, rather than the variable $\boldsymbol{x}^s$, and the relationship between $\boldsymbol{w}$ and $\boldsymbol{x}^s$ is complicated, we need to further simplify

[5]Generally, the range $[-L, L]$ is sufficient for detecting targets in the coverage of the BS. Additionally, our proposed algorithms can be easily extended to other ranges with only minor modifications.

the objective function in the following. Following the similar procedure for (20), we can obtain the following inequation, as

$$\begin{aligned}&\mathcal{R}\left\{\boldsymbol{w}^H(\boldsymbol{A}_1-\boldsymbol{B}_1)\boldsymbol{w}^{(l)}\right\}\\&=(\boldsymbol{x}^{\mathrm{c}}+\boldsymbol{x}^{\mathrm{s}})^H\left(\boldsymbol{A}_2^{(l)}-\lambda_1^{\max}(\boldsymbol{x}^{\mathrm{c}}+\boldsymbol{x}^{\mathrm{s},(l)})(\boldsymbol{x}^{\mathrm{c}}+\boldsymbol{x}^{\mathrm{s},(l)})^H\right)\\&\quad\times(\boldsymbol{x}^{\mathrm{c}}+\boldsymbol{x}^{\mathrm{s}})\\&\le 2\mathcal{R}\left\{(\boldsymbol{x}^{\mathrm{c}}+\boldsymbol{x}^{\mathrm{s},(l)})^H\Big(\boldsymbol{A}_2^{(l)}-\lambda_1^{\max}(N+L)P^{\max}\boldsymbol{I}\right.\\&\quad\left.-\lambda_2^{\max,(l)}\boldsymbol{I}\Big)(\boldsymbol{x}^{\mathrm{c}}+\boldsymbol{x}^{\mathrm{s}})\right\}+C_2^{(l)}.\end{aligned}\tag{21}$$

In the above, $\boldsymbol{A}_2^{(l)}\triangleq\sum_{n=-L}^{L}\left((r_n^{(l)})^*\boldsymbol{U}_n+(r_n^{(l)})\boldsymbol{U}_n^H\right)/2$, $\lambda_2^{\max,(l)}$ is not less than the maximum eigenvalue of $\boldsymbol{A}_2^{(l)}-\lambda_1^{\max}(N+L)P^{\max}\boldsymbol{I}$, and $C_2^{(l)}$ is a unimportant constant. Using SVD or other methods to obtain $\lambda_2^{\max,(l)}$ requires a high computational complexity. Thus, to reduce the computational complexity, $\lambda_2^{\max,(l)}$ can be set as $\max_j\sum_{i=1}^{N+L}|a_{ij}^{(l)}|$ where $a_{ij}^{(l)}$ is the element of $\boldsymbol{A}_2^{(l)}$ since $\max_j\sum_{i=1}^{N+L}|a_{ij}^{(l)}|$ is larger than the maximum eigenvalue.[6]

From the above analysis, we can finally obtain the surrogate function, as

$$\begin{aligned}\bar{f}\left(\boldsymbol{x}^{\mathrm{s}};\boldsymbol{x}^{\mathrm{s},(l)}\right)&=4\mathcal{R}\left\{(\boldsymbol{g}^{(l)})^H(\boldsymbol{x}^{\mathrm{c}}+\boldsymbol{x}^{\mathrm{s}})\right\}+C_1+2C_2^{(l)}\\&\ge f(\boldsymbol{x}^{\mathrm{s}}),\end{aligned}\tag{22}$$

where

$$\begin{aligned}\boldsymbol{g}^{(l)}\triangleq&\boldsymbol{A}_2^{(l)}(\boldsymbol{x}^{\mathrm{c}}+\boldsymbol{x}^{\mathrm{s},(l)})\\&-\left(\lambda_1^{\max}(N+L)P^{\max}+\lambda_2^{\max,(l)}\right)(\boldsymbol{x}^{\mathrm{c}}+\boldsymbol{x}^{\mathrm{s},(l)}).\end{aligned}\tag{23}$$

Then, we can solve the following optimization problem in the l-th iteration, as

$$\begin{aligned}\min_{\{\boldsymbol{x}^{\mathrm{s}},\boldsymbol{s}^{\mathrm{s}}\}}\quad&\mathcal{R}\left\{(\boldsymbol{g}^{(l)})^H(\boldsymbol{x}^{\mathrm{c}}+\boldsymbol{x}^{\mathrm{s}})\right\},\\\text{s.t.}\quad&\text{(14b) and (14c).}\end{aligned}\tag{24}$$

Although Problem (24) is not convex, the optimal solution can be derived in the following theorem.

Theorem 2. *The optimal solution to Problem (24), denoted by $\{\boldsymbol{x}^{\mathrm{s},\star},\boldsymbol{s}^{\mathrm{s},\star}\}$, can be expressed as*

$$\begin{cases}\boldsymbol{s}^{\mathrm{s},\star}=-\dfrac{\sqrt{(N+L)P^{\max}-||\boldsymbol{x}^{\mathrm{c}}||^2}(\boldsymbol{V}^{\mathrm{s}})^H\boldsymbol{g}^{(l)}}{||(\boldsymbol{V}^{\mathrm{s}})^H\boldsymbol{g}^{(l)}||},\\\boldsymbol{x}^{\mathrm{s},\star}=\boldsymbol{V}^{\mathrm{s}}\boldsymbol{s}^{\mathrm{s},\star}.\end{cases}\tag{25}$$

Proof: Please refer to Appendix B. ∎

Until now, we can solve Problem (14) using the MM method and the detailed algorithm is presented in Alg. 1. Specifically, in each iteration, we need to calculate $r_n^{(l)}$, $\boldsymbol{A}_2^{(l)}$, and $\lambda_2^{\max,(l)}$ to obtain $\boldsymbol{g}^{(l)}$ in (23). After that, Theorem 2 is used for obtaining the next iteration point $\{\boldsymbol{x}^{\mathrm{s},(l+1)},\boldsymbol{s}^{\mathrm{s},(l+1)}\}$. As we have mentioned before, the value of the objective function decreases with iteration, and thus the proposed algorithm converges to a stationary point of the original problem [44].

[6]According to [45], since $\boldsymbol{A}_2^{(l)}$ is Hermitian, its maximum eigenvalue is equal to $||\boldsymbol{A}_2^{(l)}||_2$ and is no more than the maximum absolute column sum norm, i.e., $||\boldsymbol{A}_2^{(l)}||_2\le||\boldsymbol{A}_2^{(l)}||_1=\max_j\sum_i|a_{ij}^{(l)}|$.

C. Complexity Analysis

In each iteration of the proposed MM-based algorithm, we first need to calculate $\{r_n^{(l)},n=-L,\cdots,L\}$ for $\boldsymbol{A}_2^{(l)}$ and the computational complexity is $\mathcal{O}(N(N+L))$ since calculating $r_n^{(l)}$ requires $(N+L-|n|)$ multiplications, as indicated by (7). Fortunately, the computational complexity can be reduced according to the following lemma.

Lemma 2 [46]. *For two periodic sequences $\boldsymbol{x}_1^{\mathrm{p}}\in\mathbb{C}^{n\times1}$ and $\boldsymbol{x}_2^{\mathrm{p}}\in\mathbb{C}^{n\times1}$, their cross-correlation, denoted by $\boldsymbol{r}^{\mathrm{p}}$, can be calculated by*

$$\boldsymbol{r}^{\mathrm{p}}=IDFT\{DFT\{\boldsymbol{x}_1^{\mathrm{p}}\}^*\circ DFT\{\boldsymbol{x}_2^{\mathrm{p}}\}\},\tag{26}$$

where $\circ$ is the operation of Hadamard product, and DFT$\{\cdot\}$ and IDFT$\{\cdot\}$ represent the operations of DFT and IDFT, respectively.

According to Lemma 2, we can first use $\boldsymbol{x}^{\mathrm{c}}+\boldsymbol{x}^{\mathrm{s},(l)}$ and $\boldsymbol{0}\in\mathbb{C}^{L\times1}$ to construct a periodic sequence, as $\tilde{\boldsymbol{x}}=[(\boldsymbol{x}^{\mathrm{c}}+\boldsymbol{x}^{\mathrm{s},(l)})^H\ \boldsymbol{0}^H]^H$, and calculate the autocorrelation $\tilde{r}_n$ following (26). When $n=0,1,\cdots,L$, we have

$$\tilde{r}_n=\sum_{i=0}^{N+L-n}\tilde{x}[i]^*\tilde{x}[i+n]=\sum_{i=0}^{N+L-n}x[i]^*x[i+n]=r_n.\tag{27}$$

Meanwhile, $r_n=r_{-n}^*$. Thus, $\{r_n,n=-L,\cdots,L\}$ can be extracted from $\tilde{r}_n$. The computational complexity for r_n is reduced to $\mathcal{O}((N+2L)\log(N+2L))$. Then, we need to calculate $\boldsymbol{A}_2^{(l)}$ and $\lambda_2^{\max,(l)}$, and the computational complexity can be neglected since no multiplication is needed. The next step is to obtain $\boldsymbol{g}^{(l)}$ according to (23) and the main computational complexity comes from $\boldsymbol{A}_2^{(l)}(\boldsymbol{x}^{\mathrm{c}}+\boldsymbol{x}^{\mathrm{s},(l)})$. Since $\boldsymbol{A}_2^{(l)}$ is a Toplitz matrix, $\boldsymbol{A}_2^{(l)}(\boldsymbol{x}^{\mathrm{c}}+\boldsymbol{x}^{\mathrm{s},(l)})$ is equivalent to cross-correlation between the first row of $\boldsymbol{A}_2^{(l)}$ and $\boldsymbol{x}^{\mathrm{c}}+\boldsymbol{x}^{\mathrm{s},(l)}$, and thus Lemma 2 can also be applied. The computational complexity of calculating $\boldsymbol{g}^{(l)}$ is $\mathcal{O}((N+2L)\log(N+2L))$. Besides, the computational complexity of obtaining $\{\boldsymbol{x}^{\mathrm{s},\star},\boldsymbol{s}^{\mathrm{s},\star}\}$ with Theorem 2 is $\mathcal{O}(L(N+L))$. As the maximal number of

Algorithm 1: MM-based Waveform Design Algorithm for Problem (14).

1. Initialize the maximal error tolerance $\epsilon>0$ and the maximal number of iterations $I_{\max}$;
2. Set iteration index l as 0;
3. Initialize $\boldsymbol{s}^{\mathrm{s},(0)}$ and $\boldsymbol{x}^{\mathrm{s},(0)}$;
4. **repeat**
5. Calculate $\{r_n^{(l)}\}$, $\boldsymbol{A}_2^{(l)}$, and $\lambda_2^{\max,(l)}$;
6. Calculate $\boldsymbol{g}^{(l)}$ according to (23);
7. Obtain $\{\boldsymbol{x}^{\mathrm{s},\star},\boldsymbol{s}^{\mathrm{s},\star}\}$ with Theorem 2;
8. $\boldsymbol{x}^{\mathrm{s},(l+1)}=\boldsymbol{x}^{\mathrm{s},\star}$ and $\boldsymbol{s}^{\mathrm{s},(l+1)}=\boldsymbol{s}^{\mathrm{s},\star}$;
9. $l=l+1$;
10. **until** $||\boldsymbol{s}^{\mathrm{s},(l)}-\boldsymbol{s}^{\mathrm{s},(l-1)}||\le\epsilon$ or $l>I_{\max}$.

iterations is $I_{\max}$, the total computational complexity of the proposed MM-based algorithm is

$$\mathcal{O}\left(I_{\max}\left(L(N+L)+(N+2L)\log(N+2L)\right)\right). \quad (28)$$

The convergence speed of the MM method highly depends on the surrogate function. To accelerate convergence, the squared iterative method (SQUAREM) can be further utilized and the main idea is to use two consecutive iterations to find a faster direction of descent [47].

IV. Low-complexity Waveform Design

The MM-based waveform design algorithm in the previous section can improve the sensing performance without degrading the communication performance. However, in some practical scenarios with the requirement of low latency, it fails to meet the latency requirements due to the need for multiple iterations to converge. Therefore, this section proposes a low-complexity waveform design method to address the low latency challenge. It is noteworthy that the previous section directly aims at minimizing the sensing performance and adopts an iterative strategy to achieve the goal. Hence, to reduce the computational complexity, this section proposes a completely new waveform design approach. The simplest idea is to directly superimpose a signal with high sensing performance on the communication signal. However, this approach often performs poorly since the sensing signal is not solely designed for the given communication signal. Therefore, the solution proposed in this section aims to further enhance the sensing performance based on this. The main idea is to first analyze the intrinsic characteristics of high-performance sensing signals and then optimize the sensing signal based on the intrinsic characteristics. The specific design approach is divided into three steps:

- **Step 1**: Generate a pure sensing signal, denoted by $\boldsymbol{x}^{\mathrm{s},\star}$, by solving Problem (14) using Alg. 1 with $\boldsymbol{x}^{\mathrm{c}}=\mathbf{0}$.
- **Step 2**: Construct the transmit signal. Find the optimal combination between $\boldsymbol{x}^{\mathrm{c}}$ and $\boldsymbol{x}^{\mathrm{s},\star}$ to construct the transmit signal, denoted by $\boldsymbol{x}^{\mathrm{in}}$.
- **Step 3**: Optimize the transmit signal. Enhance the sensing performance of the transmit signal by optimizing the sensing signal. First, explore the intrinsic characteristics of high sensing performance signals, then select the appropriate target signal $\boldsymbol{x}^{\mathrm{tar}}$, and finally select the best $\boldsymbol{x}^{\mathrm{fin}}$ to make the final transmit signal as close to $\boldsymbol{x}^{\mathrm{tar}}$ as possible.

In the above, $\boldsymbol{x}^{\mathrm{s},\star}$ in **Step 1** only needs to be generated once during the channel correlation time since $\boldsymbol{V}^{\mathrm{s}}$ remains unchanged during the channel correlation time. Thus, the computational complexity of **Step 1** can be ignored. Hence, we elaborate more details on **Step 2** and **Step 3**.

A. Construct Transmit Signal

In this section, we opt to superimpose $\boldsymbol{x}^{\mathrm{c}}$ with $e^{i\theta}\boldsymbol{x}^{\mathrm{s},\star}$, where $e^{i\theta}$ is optimized to further improve the sensing performance. The autocorrelation of $\boldsymbol{x}^{\mathrm{c}}+e^{i\theta}\boldsymbol{x}^{\mathrm{s},\star}$ can be expressed as

$$\begin{aligned}\hat{f}(\theta)&=\sum_{n=-L}^{L}|r_n|^2\\&=2\mathcal{R}\left\{e^{i2\theta}D_1\right\}+4\mathcal{R}\left\{e^{i\theta}D_2\right\}+D_3,\end{aligned} \quad (29)$$

where $D_1=\sum_{n=-L}^{L}|b_n|^2$, $D_2=\sum_{n=-L}^{L}a_nb_n$, $D_3=\sum_{n=-L}^{L}|a_n|^2+2|b_n|^2$, $a_n=(\boldsymbol{x}^{\mathrm{c}})^H\boldsymbol{U}_n\boldsymbol{x}^{\mathrm{c}}+(\boldsymbol{x}^{\mathrm{s},\star})^H\boldsymbol{U}_n\boldsymbol{x}^{\mathrm{s},\star}$, and $b_n=(\boldsymbol{x}^{\mathrm{c}})^H\boldsymbol{U}_n\boldsymbol{x}^{\mathrm{s},\star}$. We aim to minimize $\hat{f}(\theta)$ and the optimal solution, denoted by $\theta^\star$, is given in the following theorem.

Theorem 3. *The optimal solution to minimize $\hat{f}(\theta)$ is*

$$\theta^\star=\begin{cases}0, & D_2\le -2D_1,\\ \pi, & D_2\ge 2D_1,\\ \arccos\left(-D_2/(2D_1)\right), & \text{otherwise.}\end{cases} \quad (30)$$

Proof: Please refer to Appendix C. ∎

According to Theorem 3, the constructed primary transmit signal is

$$\boldsymbol{x}^{\mathrm{in}}=\boldsymbol{x}^{\mathrm{c}}+e^{i\theta^\star}\boldsymbol{x}^{\mathrm{s},\star}. \quad (31)$$

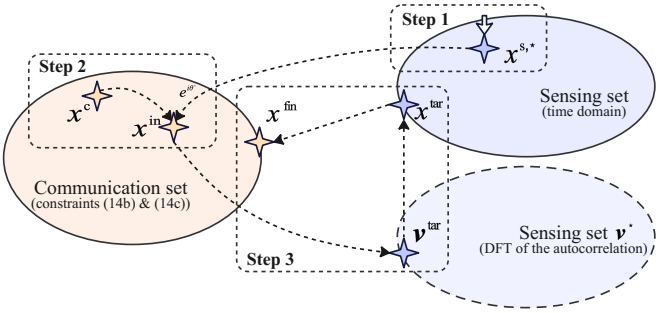

Fig. 3. The illustration of transmit signal optimization.

B. Optimize Transmit Signal

Since $\boldsymbol{x}^{\mathrm{s},\star}$ is generated in advance and not solely designed for improving the sensing performance of $\boldsymbol{x}^{\mathrm{c}}$, the improvement of the sensing performance is limited. To further improve it, directly optimizing $\boldsymbol{x}^{\mathrm{in}}$ is not advisable, which generally needs iteration. Instead, as shown in Fig. 3, we first analyze the characteristics of the high-performance sensing signals and construct the sensing set for these signals. Then, the one closest to $\boldsymbol{x}^{\mathrm{in}}$ (i.e., $\boldsymbol{x}^{\mathrm{tar}}$) is picked out from the sensing set. Finally, in the communication set formed by constraints (14b) and (14c), we select the final transmit signal, denoted by $\boldsymbol{x}^{\mathrm{fin}}$, that is the closest to $\boldsymbol{x}^{\mathrm{tar}}$.

However, it is hard to analyze the characteristic of the signal with high sensing performance using the transmit signal $\boldsymbol{x}$ since the autocorrelation in (7) is very complicated. Inspired by the relationship between the DFT of a periodic sequence and that of its autocorrelation in Lemma 2, we can first analyze the DFT of the autocorrelation and then use its characteristic to design the transmit signal. Specifically, as we have mentioned before, to calculate $\{r_n, n=-L,\cdots,L\}$, the length of the sequence should be $N+2L$. Thus, the DFT of the autocorrelation can be denoted as $\boldsymbol{\nu}\in\mathbb{R}^{(N+2L)\times 1}$. Note that the value of each

element in $\boldsymbol{\nu}$ is not less than zero since the DFT of the autocorrelation is the absolute square of the DFT of the sequence. The autocorrelation r_n can be expressed as $\boldsymbol{f}_n^H\boldsymbol{\nu}/(N+2L)$, where $\boldsymbol{f}_n = \left[1, e^{\frac{-i2\pi n}{N+2L}}, \cdots, e^{\frac{-i2\pi n(N+2L-1)}{N+2L}}\right]^T \in \mathbb{C}^{(N+2L)\times 1}$. The problem for maximizing the sensing performance can be formulated as

$$\min_{\boldsymbol{\nu}} \quad \sum_{n=-L}^{L} |r_n|^2 = \sum_{n=-L}^{L} ||\boldsymbol{f}_n^H\boldsymbol{\nu}||^2/(N+2L)^2, \tag{32a}$$

$$\text{s.t.} \quad \mathbf{1}^T\boldsymbol{\nu} = (N+2L)P^{\max}, \tag{32b}$$

$$\boldsymbol{\nu} \geq \mathbf{0}, \tag{32c}$$

where $\mathbf{1} = [1, \cdots, 1]^T \in \mathbb{R}^{(N+2L)\times 1}$ and the constraint (32b) limits the total transmit power, derived from (14c). The optimal solution can be presented in the following theorem.

Theorem 4. *The optimal solution to Problem (32) is*

$$\boldsymbol{\nu}^\star = P^{\max}\mathbf{1} + \boldsymbol{F}_{R,2}\boldsymbol{\phi} \geq \mathbf{0}, \tag{33}$$

where $\boldsymbol{F}_{R,2} = [\mathcal{R}\{\boldsymbol{f}_{L+1}\}, \mathcal{I}\{\boldsymbol{f}_{L+1}\}, \cdots, \mathcal{R}\{\boldsymbol{f}_{N/2+L-1}\}, \mathcal{I}\{\boldsymbol{f}_{N/2+L-1}\}] \in \mathbb{R}^{(N+2L)\times(N-1)}$ *and* $\boldsymbol{\phi} \in \mathbb{R}^{(N-1)\times 1}$ *could be any vector that satisfies* $\boldsymbol{\nu}^\star \geq \mathbf{0}$*. Consequently, the optimal value to Problem (32) is* $(P^{\max})^2$ *and* $r_n = 0$*,* $n = \{-L, \cdots, -1, 1 \cdots, L\}$.

Proof: Please refer to Appendix D. ∎

Theorem 4 forms the ideal sensing set of the autocorrelation's DFT for a sequence with high sensing performance. Intuitively, $\boldsymbol{x}$ needs to approach this set if we want to improve its sensing performance. To this end, we can select a sequence $\boldsymbol{x}^{\text{tar}}$ from the set that is the closest to the constructed primary transmit signal $\boldsymbol{x}^{\text{in}}$. After that, we derive the final transmit signal from $\boldsymbol{x}^{\text{tar}}$. Thus, let $\boldsymbol{\nu}^{\text{in}}$ denote the autocorrelation's DFT of $\boldsymbol{x}^{\text{in}}$, and the optimization problem for finding the autocorrelation's DFT of $\boldsymbol{x}^{\text{tar}}$, denoted by $\boldsymbol{\nu}^{\text{tar}}$, can be formulated as

$$\min_{\{\boldsymbol{\nu},\boldsymbol{\phi}\}} \quad ||\boldsymbol{\nu} - \boldsymbol{\nu}^{\text{in}}||^2, \tag{34a}$$

$$\text{s.t.} \quad \boldsymbol{\nu} = P^{\max}\mathbf{1} + \boldsymbol{F}_{R,2}\boldsymbol{\phi}, \tag{34b}$$

$$\boldsymbol{\nu} \geq \mathbf{0}. \tag{34c}$$

Since this problem is convex, the closed-form optimal solution can be derived as

$$\boldsymbol{\nu}^{\text{tar}} = P^{\max}\mathbf{1} + \boldsymbol{F}_{R,2}\boldsymbol{F}_{R,2}^T\left(\boldsymbol{\lambda}_2 + \boldsymbol{\nu}^{\text{in}} - P^{\max}\mathbf{1}\right), \tag{35}$$

where $\boldsymbol{\lambda}_2$ is the Lagrangian parameter that satisfies $\boldsymbol{\nu}^{\text{tar}} \geq \mathbf{0}$. The details can be found in Appendix E.

Due to the existence of $\boldsymbol{\lambda}_2$, we need to apply the exhaustive searching algorithm to find $\boldsymbol{\nu}^{\text{tar}}$, which may increase the computational complexity. To avoid this, we directly use a sub-optimal solution, which is simplified from (35), as

$$\begin{aligned}\boldsymbol{\nu}^{\text{tar}} =& P^{\max}\mathbf{1} + \boldsymbol{F}_{R,2}(\boldsymbol{F}_{R,2})^T \\ &\times (\boldsymbol{F}_{R,2}(\boldsymbol{F}_{R,2})^T(\boldsymbol{\nu}^{\text{in}} - P^{\max}\mathbf{1}) + P^{\max}\mathbf{1})^+,\end{aligned} \tag{36}$$

where $(\boldsymbol{a})^+$ represents the element-wise operation that sets the element in $\boldsymbol{a}$ to be zero if it is negative. Then, the corresponding $\boldsymbol{x}^{\text{tar}}$ can be derived with the operations of square root and IDFT, as

$$\boldsymbol{x}^{\text{tar}} = (\boldsymbol{F}^{\text{part}})^H \text{Diag}\{\boldsymbol{\phi}\}\sqrt{\boldsymbol{\nu}^{\text{tar}}}, \tag{37}$$

where $\sqrt{\boldsymbol{\nu}^{\text{tar}}}$ represents the square root operation on each element of $\boldsymbol{\nu}^{\text{tar}}$, $\boldsymbol{\phi} = [e^{i\phi_n}] \in \mathbb{C}^{(N+L)\times 1}$ is the phase vector, and $\text{Diag}\{\boldsymbol{\phi}\} \in \mathbb{C}^{(N+2L)\times(N+2L)}$ is the matrix with the diagonal being $\boldsymbol{\phi}$ and other elements being zeros. To force $\boldsymbol{x}^{\text{tar}}$ be close to $\boldsymbol{x}^{\text{in}}$, the phase of each element in $\boldsymbol{x}^{\text{tar}}$ should be the same as that in $\boldsymbol{x}^{\text{in}}$. Thus, $\boldsymbol{\phi}$ should be

$$\boldsymbol{\phi} = \angle(\boldsymbol{F}^{\text{part}}\boldsymbol{x}^{\text{in}}). \tag{38}$$

Until now, we have obtained a sequence $\boldsymbol{x}^{\text{tar}}$ with good sensing performance and it is close to $\boldsymbol{x}^{\text{in}}$. However, as $\boldsymbol{x}^{\text{tar}}$ does not satisfy the communication requirement, i.e., no degradation on the communication performance, it cannot be directly used for transmission. Instead, we can redesign $\boldsymbol{x}^{\text{s}}$ to force $\boldsymbol{x}$ to approach $\boldsymbol{x}^{\text{tar}}$ under the consideration of the transmit power limitation (14c). Thus, denoting $\boldsymbol{x}^{\text{s,fin}}$ as the optimized $\boldsymbol{x}^{\text{s}}$, we have

$$\boldsymbol{x}^{\text{s,fin}} = \frac{\sqrt{(N+L)P^{\max} - ||\boldsymbol{x}^{\text{c}}||^2}\boldsymbol{V}^{\text{s}}(\boldsymbol{V}^{\text{s}})^H(\boldsymbol{x}^{\text{tar}} - \boldsymbol{x}^{c})}{||(\boldsymbol{V}^{\text{s}})^H(\boldsymbol{x}^{\text{tar}} - \boldsymbol{x}^{\text{c}})||}. \tag{39}$$

Then, the final transmit signal is

$$\boldsymbol{x}^{\text{fin}} = \boldsymbol{x}^{\text{c}} + \boldsymbol{x}^{\text{s,fin}}. \tag{40}$$

C. Summary of the Low-Complexity Algorithm

The overall low-complexity waveform design algorithm is presented in Alg. 2. There is no iteration in the low-complexity algorithm and the computational complexity mainly comes from the matrix multiplication. There are two types of matrix multiplication: one is for DFT or IDFT, and the other is related to $\boldsymbol{V}^{\text{s}}$, e.g., $(\boldsymbol{V}^{\text{s}})^H(\boldsymbol{x}^{\text{tar}} - \boldsymbol{x}^{\text{c}})$ in (39). Their computational complexity is $\mathcal{O}\left((N+2L)\log(N+2L)\right)$ and $\mathcal{O}\left(L(N+L)\right)$, respectively. Therefore, the total computational complexity of the low-complexity algorithm is

$$\mathcal{O}\left(L(N+L) + (N+2L)\log(N+2L)\right). \tag{41}$$

Compared to the MM-based algorithm, the computational complexity of Alg. 2 is much lower, approaching the computational complexity of the fast Fourier transform (FFT) operation, i.e., $\mathcal{O}\left(N\log(N)\right)$. Thus, Alg. 2 can satisfy the latency requirement in practical systems.

Algorithm 2: Low-Complexity Waveform Design Algorithm.

1. **Input**: The pure sensing signal $\boldsymbol{x}^{\text{s},\star}$ and the communication signal $\boldsymbol{x}^{\text{c}}$;
2. Find $\theta^\star$ according to Theorem 3 and calculate $\boldsymbol{x}^{\text{in}}$;
3. Calculate $\boldsymbol{\nu}^{\text{tar}}$ with (36);
4. Calculate $\boldsymbol{x}^{\text{tar}}$ with (37);
5. Calculate $\boldsymbol{x}^{\text{s,fin}}$ with (39);
6. **Output**: $\boldsymbol{x}^{\text{fin}} = \boldsymbol{x}^{\text{c}} + \boldsymbol{x}^{\text{s,fin}}$.

TABLE I
SIMULATION PARAMETERS

Parameter	Value
Data length, N	128
CP length, L	32
Communication power, P^{c}	1 W
Sensing power, ΔP	1 W
False alarm rate	10^{-5}
SNR of the strong target	3 dB
SNR of the weak target	-7 dB

V. SIMULATION RESULTS

In this section, we present simulation results to validate the performance of the proposed algorithms.

A. Simulation Setup

The simulation settings are summarized as follows unless otherwise specified. The length of the transmit data is 128, i.e., $N = 128$, and the length of the CP is 32, i.e., $L = 32$. The transmit power for communication is 1 W, i.e., $P^{\mathrm{c}} = 1$ W, and the additional power for sensing is also 1 W, i.e., $\Delta P = 1$ W. Thus, the total transmit power upper bound $P^{\max}$ is 2 W. For the communication part, each element in the wireless channel vector $\boldsymbol{h}$ between the dual-functional BS and the user follows complex Gaussian distribution with the mean being zero and variance being $1/(L+1)$, i.e., $h_l \sim \mathcal{CN}\left(0, \frac{1}{L+1}\right)$, $l = 1, \cdots, L+1$. For the sensing part, we assume that there are two targets distributed within the area, i.e., a strong one and a weak one. The echo SNR for the strong target is 3 dB, while for the weak target, it is -7 dB. The time difference between the echoes of the two targets is $\lfloor L/3 \rfloor + 4$. The received echoes are detected using the cell averaging (CA)-CFAR method [46], with one protection cell and a reference cell length of $\lfloor L/4 \rfloor$, and the false alarm rate is set as 10^{-5}. The main parameters are listed in Tab. I.

To demonstrate the impact of sidelobe levels and the effectiveness of the proposed algorithms, this section uses the detection probability of the weak target for illustration. It is noteworthy that by controlling the echo SNR as a constant, performance differences caused by the power increase can be excluded.

B. Algorithm Investigation

We first pay attention to the convergence behavior of the MM-based waveform design algorithm (Alg. 1). The variations of the objective function in (12) and the corresponding decline after one iteration are shown in Fig. 4. Note that we adopt the SQUAREM to accelerate the convergence of the proposed algorithm. From Fig. 4, the algorithm almost converges to a stationary point within 20 iterations as the decline is less than 10^{-3}. Moreover, the decline of the iteration is less than 10^{-4} when the number of iteration is 40. These results verify the fast convergence of the proposed MM-based algorithm. Meanwhile, the final objective value is almost zero, which means that the sidelobe level is almost zero. It demonstrates the high sensing performance of the MM-based algorithm.

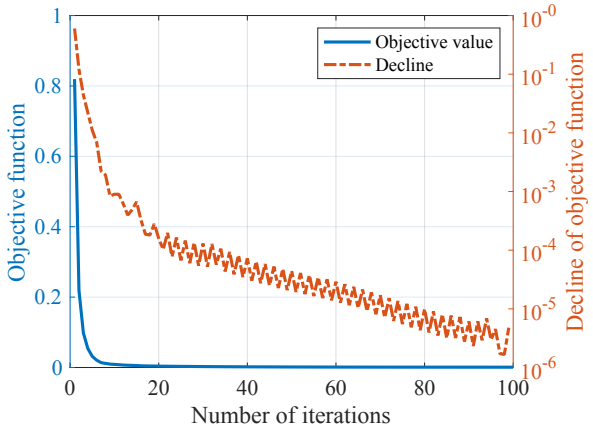

Fig. 4. Convergence behavior of the MM-based algorithm.

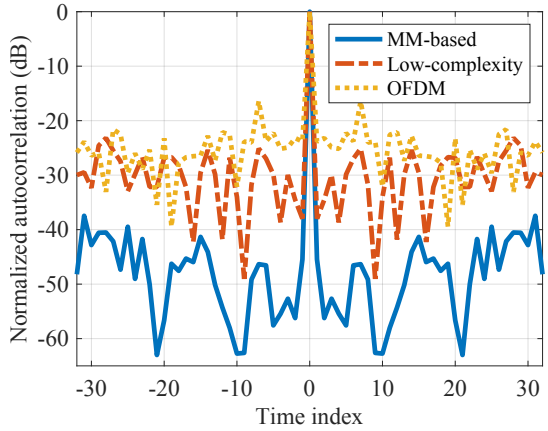

Fig. 5. Normalized autocorrelation of three schemes.

We also compare the running time and sensing performance of the proposed MM-based algorithm under different error tolerances with the low-complexity algorithm, and the results are shown in Tab. II. Note that both algorithms are implemented using MATLAB on a desktop Intel (i5-13600K) CPU running at 3.5 GHz with 24 GB RAM. It can be observed that the running time of the MM-based algorithm is at the millisecond level while that of the low-complexity algorithm is at the microsecond level. Thus, the MM-based algorithm can be used in most communication scenarios and the low-complexity algorithm can be used in the real-time communication scenario that demands ultra-low latency. Meanwhile, the objective values achieved by both algorithms are very close to 0, with the MM-based algorithm achieving a value even closer to 0. This result verifies the good sensing performance of both algorithms.

C. Performance Comparison

In this section, we aim to compare the sensing performance of the proposed algorithms to that of the conventional OFDM waveform. First of all, Fig. 5 shows the normalized autocorrelation of the transmit signal in three schemes. It can be observed that the sidelobe level of the autocorrelation during the range to be optimized (from $-L$ to L) can be reduced with our proposed algorithms. The MM-based algorithm achieves the best sensing performance. Note that a lower sidelobe level

TABLE II
RUNNING TIME AND SENSING PERFORMANCE COMPARISON

Algorithm	MM-based algorithm			Low-complexity algorithm
Error tolerance	10^{-4}	10^{-5}	10^{-6}	
Running time (second)	2.7×10^{-3}	3.0×10^{-3}	5.8×10^{-3}	5.4×10^{-5}
Objective value	4.0×10^{-4}	4.0×10^{-4}	4.0×10^{-4}	9.1×10^{-3}

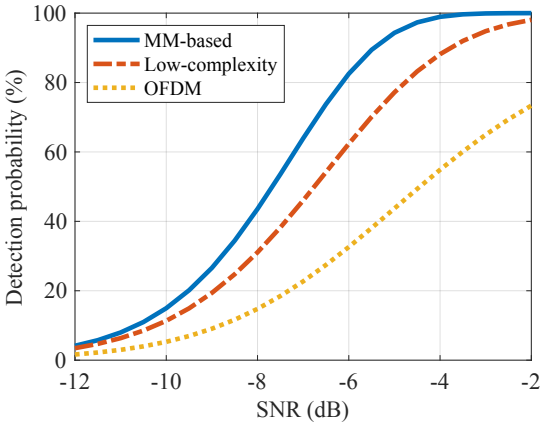

Fig. 6. Detection probability versus SNR of the weak target.

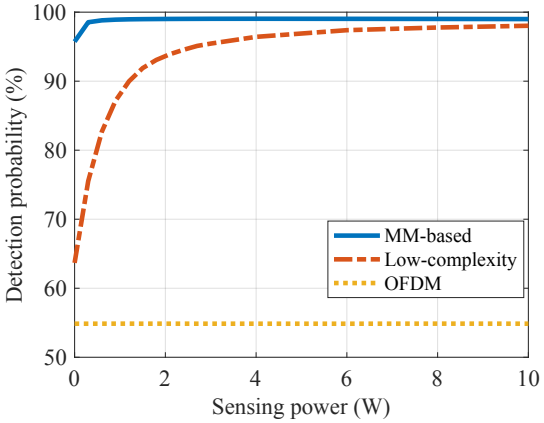

Fig. 7. Detection probability versus sensing power.

means a higher detection probability. To further demonstrate the sensing performance of the two algorithms, we will show the detection probability of the weak target in the following.

Fig. 6 shows the relationship between the detection probability and the echo SNR for the weak target. Notably, the corresponding strong target's echo SNR is always 10dB higher than that of the weak target. The figure demonstrates that the detection probability continually rises as the SNR increases. Moreover, the proposed algorithms can indeed enhance the sensing performance. It is important to note that the proposed scheme does not affect the communication performance at all. The performance of the MM-based algorithm is the best since it converges to a stationary solution. Furthermore, the low-complexity algorithm trades sensing performance for less running time, with the sensing performance lying between those of the MM-based algorithm and the original OFDM data signal. Additionally, the performance gain becomes more pronounced as the SNR increases. To achieve the detection probability of about 60 %, the low-complexity algorithm

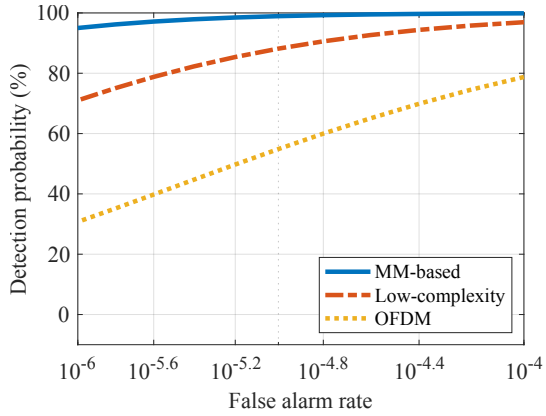

Fig. 8. Detection probability versus false alarm rate.

requires about 2.4 dB less than the original OFDM signals. Moreover, the performance gap becomes larger as the SNR increases. Notably, the main factor affecting the weak target's detection probability at high SNR levels is the sidelobe of the strong target's autocorrelation since the noise power is relatively low. Therefore, the performance gap at high SNR levels suffices to demonstrate that the proposed MM-based and low-complexity algorithms can effectively mitigate interference between different targets, thereby enhancing the sensing performance.

Fig. 7 shows the relationship between the detection probability of the weak target and the sensing power. It is important to note that since the echo SNR of the weak target is fixed, increasing sensing power only affects the relative power of $\boldsymbol{x}^{\mathrm{c}}$ and $\boldsymbol{x}^{\mathrm{s}}$. The sensing performance can be improved even without adding extra sensing power. It is because part of the signal, i.e., $(\boldsymbol{V}^{\mathrm{s}})^H \boldsymbol{V}^{\mathrm{s}} \boldsymbol{x}^{\mathrm{o,c}}$, is ineffective for communication. Utilizing this portion of power for sensing can significantly improve the sensing performance. Even when the sensing power is low, the MM-based algorithm reaches its performance limit. Note that the increase of the sensing power would not influence the SNR gap between the strong target and the weak target. Thus, the main factor hindering the increase in detection probability for the MM-based algorithm is channel noise when the sensing power is low. The above results indicate that the MM-based algorithm can achieve good sensing performance with a low power expenditure. Furthermore, the sensing performance of the low-complexity algorithm also increases with sensing power. Because it heuristically superimposes the existing sensing signal on the communication signal, its performance is relatively worse than the MM-based algorithm. Moreover, it also approaches the performance of the MM-based algorithm when the sensing power is high.

Fig. 8 shows the relationship between the detection proba-

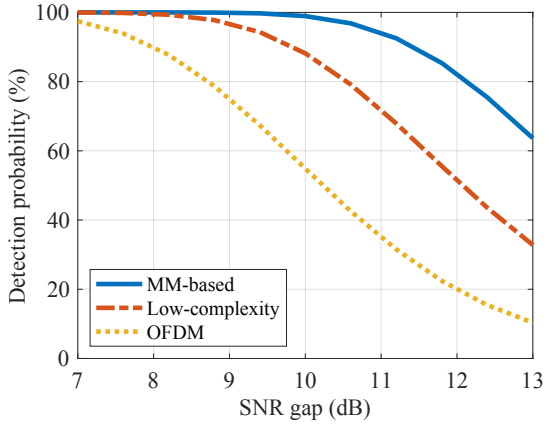

Fig. 9. Detection probability versus SNR gap.

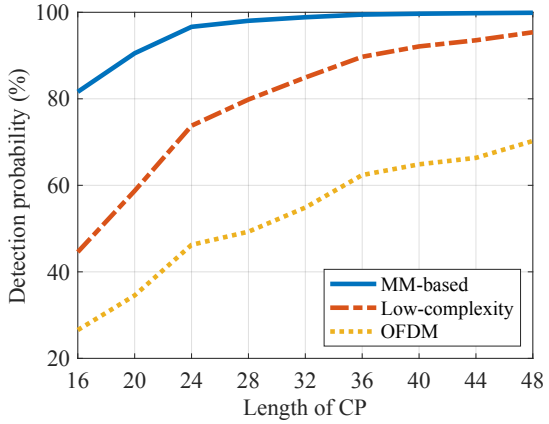

Fig. 10. Detection probability versus CP length.

bility of the weak target and the false alarm rate. The figure illustrates that the detection probability also rises as the false alarm rate increases. This is because a higher false alarm rate implies a lower threshold for detecting the echo from a potential target, thereby the detection probability increases. In practice, the false alarm rate can be set according to the detection probability requirement.

Fig. 9 plots the effect of the SNR gap between the strong target and the weak target on the detection probability. Note that the SNR of the strong target remains constant, i.e., 3 dB, and we vary the SNR of the weak target to control the SNR gap. The increase of the SNR gap means the decrease of the weak target's SNR. Thus, the detection probability of the weak target decreases with the SNR gap. When the SNR gap is low, all three schemes can achieve almost 100 % detection probability. As the SNR gap increases, the superiority of the proposed MM-based and low-complexity algorithms begins to emerge gradually since the autocorrelation's sidelobe of the two algorithms is much lower than that of the conventional OFDM waveform.

Fig. 10 shows the relationship between the detection probability of the weak target and the length of the CP. From the figure, it can be observed that the longer the CP is, the higher the detection probability of the weak target will be. This is because a longer CP means a longer sequence length of the transmit signal, which in turn leads to lower sidelobe intensity, making it less likely for the autocorrelation's peak of the weak target echo to be masked by the autocorrelation's sidelobes of the strong target echo. Moreover, compared with the original OFDM communication signal, the performance of the low-complexity algorithm increases faster as the CP length increases, since a longer CP provides more freedom for the sensing signal optimization, thereby bringing more significant performance improvements.

VI. Conclusion

In this paper, we have proposed a novel dual-functional waveform design method that contains a novel null-space sensing precoder. The precoder is used for projecting the additional sensing signals into the null space of the wireless channel. Thus, the proposed waveform design method can enhance the sensing performance without degrading the communication performance. A waveform optimization problem has been formulated for maximizing the sensing performance with the null-space sensing precoder and the constraint of maximum transmit power. To solve it, we have proposed an MM-based algorithm that converges to a stationary point of the formulated problem. Considering the real-time communication requirement in practice, we have also developed a low-complexity algorithm based on the analysis on the intrinsic characteristics of the high-performance sensing signals. Finally, numerical results have been presented to verify the effectiveness of two proposed algorithms. Results show that the MM-based algorithm significantly improves the sensing performance without additional sensing power, and the low-complexity algorithm requires much reduced computational complexity for substantial improvements in the sensing performance.

Our initial study in this work has demonstrated the effectiveness of the null-space sensing precoder and the corresponding ISAC waveform design method. In our future work, we will further develop some practical techniques to facilitate the implementation of the proposed waveform design. First, the proposed null-space sensing precoder relies on the perfect channel estimation. To meet the channel estimation error in practice, we will further develop robust waveform design methods based on several existing works, e.g., [48]. Secondly, we only consider the single-input single-output (SISO) system in this paper. For the multiple-input multiple-output (MIMO) system, the null-space sensing precoder still works due to the existence of CP, and the proposed waveform design algorithm can be extended, which we leave as our future exploration.

Appendix A
Details for Deriving (18)

First of all, we have

$$\begin{aligned} f(\boldsymbol{x}^{\mathrm{s}}) &= \sum_{n=-L}^{L} \left|\mathrm{tr}\left\{(\boldsymbol{x}^{\mathrm{c}}+\boldsymbol{x}^{\mathrm{s}})(\boldsymbol{x}^{\mathrm{c}}+\boldsymbol{x}^{\mathrm{s}})^H \boldsymbol{U}_n\right\}\right|^2 \\ &\overset{(a)}{=} \sum_{n=-L}^{L} \left|\mathrm{vec}\left\{(\boldsymbol{x}^{\mathrm{c}}+\boldsymbol{x}^{\mathrm{s}})(\boldsymbol{x}^{\mathrm{c}}+\boldsymbol{x}^{\mathrm{s}})^H\right\}^H \mathrm{vec}\left\{\boldsymbol{U}_n\right\}\right|^2 \\ &\overset{(b)}{=} \boldsymbol{w}^H \left(\sum_{n=-L}^{L} \mathrm{vec}\left\{\boldsymbol{U}_n\right\} \mathrm{vec}\left\{\boldsymbol{U}_n\right\}^H\right) \boldsymbol{w}, \end{aligned} \tag{42}$$

where (a) is derived from an identity equation $\text{tr}\left\{\boldsymbol{A}^H\boldsymbol{B}\right\} = \text{vec}\{\boldsymbol{A}\}^H \text{vec}\{\boldsymbol{B}\}$ and (b) is obtained by defining $\boldsymbol{w} \triangleq \text{vec}\left\{(\boldsymbol{x}^{\text{c}}+\boldsymbol{x}^{\text{s}})(\boldsymbol{x}^{\text{c}}+\boldsymbol{x}^{\text{s}})^H\right\}$. Then, with defining $\boldsymbol{A}_1 \triangleq \sum_{n=-L}^{L} \text{vec}\{\boldsymbol{U}_n\}\text{vec}\{\boldsymbol{U}_n\}^H$ and $\boldsymbol{B}_1$ that satisfies $\boldsymbol{B}_1 \succeq \boldsymbol{A}_1$, we can apply Lemma 1 and obtain inequation (18).

APPENDIX B
PROOF OF THEOREM 2

With constraint (14b), the objective function can be rewritten as

$$\mathcal{R}\left\{(\boldsymbol{g}^{(l)})^H(\boldsymbol{x}^{\text{c}}+\boldsymbol{V}^{\text{s}}\boldsymbol{s}^{\text{s}})\right\}, \tag{43}$$

which is a linear function. To minimize it, the direction of $\boldsymbol{s}^{\text{s}}$ should be the same as that of $-(\boldsymbol{V}^{\text{s}})^H\boldsymbol{g}^{(l)}$. Meanwhile, there is a limitation of the total transmit power (14c). Thus, the optimal solution can be expressed as shown in (25), which ends the proof.

APPENDIX C
PROOF OF THEOREM 3

First, $\hat{f}(\theta)$ can be rewritten as

$$\begin{aligned}\hat{f}(\theta) &= 2D_1\cos(2\theta) + 4D_2\cos(\theta) + D_3\\ &= 4D_1(\cos(\theta))^2 + 4D_2\cos(\theta) + D_3 - 2D_1\\ &= 4D_1z^2 + 4D_2z + D_3 - 2D_1,\end{aligned} \tag{44}$$

which is a quadratic function with $z = \cos(\theta) \in [-1,1]$. Note that $D_1 > 0$ and thus the minimum of $\hat{f}(\theta)$ can be achieved when z is $-D_2/(2D_1)$ if z has no range constraint. Since $z \in [-1,1]$, there exist three cases:

- When $-D_2/(2D_1) \in [-1,1]$, the optimal z is $-D_2/(2D_1)$. Hence, $\theta^\star = \arccos(-D_2/(2D_1))$;
- When $D_2 > 2D_1$, the optimal z is -1. In this case, $\theta^\star = \pi$;
- When $D_2 < -2D_1$, the optimal z is 1. In this case, $\theta^\star = 0$.

Therefore, the optimal solution for minimizing $\hat{f}(\theta)$ can be concluded in (30), which ends the proof.

APPENDIX D
PROOF OF THEOREM 4

The objective function can be rewritten as

$$\begin{aligned}&\sum_{n=-L}^{L} ||\boldsymbol{f}_n^H\boldsymbol{\nu}||^2/(N+2L)^2\\ &= \frac{\sum_{n=-L}^{L}\left((\mathcal{R}\{\boldsymbol{f}_n\}^H\boldsymbol{\nu})^2 + (\mathcal{I}\{\boldsymbol{f}_n\}^H\boldsymbol{\nu})^2\right)}{(N+2L)^2}\\ &= (P^{\max})^2 + \frac{\sum_{n=1}^{L} 2\left((\mathcal{R}\{\boldsymbol{f}_n\}^H\boldsymbol{\nu})^2 + (\mathcal{I}\{\boldsymbol{f}_n\}^H\boldsymbol{\nu})^2\right)}{(N+2L)^2}.\end{aligned} \tag{45}$$

In the above, (45) is derived based the fact: $(\mathcal{R}\{\boldsymbol{f}_n\}^H\boldsymbol{\nu})^2 + (\mathcal{I}\{\boldsymbol{f}_n\}^H\boldsymbol{\nu})^2 = (\mathcal{R}\{\boldsymbol{f}_{-n}\}^H\boldsymbol{\nu})^2 + (\mathcal{I}\{\boldsymbol{f}_{-n}\}^H\boldsymbol{\nu})^2$. To minimize the objective function, $\boldsymbol{\nu}$ should be orthogonal to both $\mathcal{R}\{\boldsymbol{f}_n\}$ and $\mathcal{I}\{\boldsymbol{f}_n\}$, $\forall n \in \{1,\cdots,L\}$. Meanwhile, it can be found that $\mathcal{R}\{\boldsymbol{f}_n\}$ and $\mathcal{I}\{\boldsymbol{f}_n\}$, $\forall n \in \{0,\cdots,N/2+L-1\}$ are orthogonal to each other. Therefore, $\boldsymbol{\nu}$ should be the linear combination of $\mathcal{R}\{\boldsymbol{f}_n\}$ and $\mathcal{I}\{\boldsymbol{f}_n\}$, $\forall n \in \{0, L+1,\cdots,N/2+L-1\}$ for minimizing the objective function. Note that $\mathbf{1}^T\mathcal{R}\{\boldsymbol{f}_n\} = 0$, $\forall n \in \{1,\cdots,N/2+L-1\}$, and $\mathbf{1}^T\mathcal{I}\{\boldsymbol{f}_n\} = 0, \forall n \in \{0,1,\cdots,N/2+L-1\}$. Thus, to satisfy the power constraint (32b), the coefficient of $\mathcal{R}\{f_0\}$ (i.e., $\mathbf{1} \in \mathbb{R}^{(N+L)\times 1}$) should be $P^{\max}$ in the linear combination for $\boldsymbol{\nu}$. Furthermore, with constraint (32c), the optimal solution to Problem (32) is expressed as (33), which ends the proof.

APPENDIX E
DETAILS FOR SOLVING PROBLEM (34)

In Problem (34), the objective function is quadratic and all constraints are linear. Thus, Problem (34) is convex, and we can utilize the Lagrange multiplier method. The Lagrange function for Problem (34) can be expressed as

$$\begin{aligned}\mathcal{L} =&||\boldsymbol{\nu}-\boldsymbol{\nu}^{\text{in}}||^2 + \boldsymbol{\lambda}_2^T\boldsymbol{\nu}\\ &+ \boldsymbol{\lambda}_1^T\left(P^{\max}\mathbf{1} + \boldsymbol{F}_{R,2}\boldsymbol{\phi} - \boldsymbol{\nu}\right) + \boldsymbol{\lambda}_2^T\boldsymbol{\nu},\end{aligned} \tag{46}$$

where $\boldsymbol{\lambda}_1$ and $\boldsymbol{\lambda}_2$ are the Lagrange multipliers associated with the constraints (34b) and (34c). Then, the necessary and sufficient conditions based on the Karush-Kuhn-Tucker (KKT) conditions can be expressed as

$$\frac{\partial\mathcal{L}}{\partial\boldsymbol{\nu}} = 2(\boldsymbol{\nu}-\boldsymbol{\nu}^{\text{in}}) - \boldsymbol{\lambda}_1 + \boldsymbol{\lambda}_2 = \mathbf{0}, \tag{47}$$

$$\frac{\partial\mathcal{L}}{\partial\boldsymbol{\phi}} = \boldsymbol{F}_{R,2}^T\boldsymbol{\lambda}_1 = \mathbf{0}, \tag{48}$$

$$\boldsymbol{\lambda}_1^T\left(P^{\max}\mathbf{1} + \boldsymbol{F}_{R,2}\boldsymbol{\phi} - \boldsymbol{\nu}\right) = 0, \tag{49}$$

$$\boldsymbol{\lambda}_2^T\boldsymbol{\nu} = 0, \quad \boldsymbol{\lambda}_2 \geq \mathbf{0}. \tag{50}$$

With simple mathematical analysis and calculations, we can derive the optimal solution in (35). This ends the proof.

REFERENCES

[1] B. Rong, "6G: The next horizon: From connected people and things to connected intelligence," *IEEE Wireless Commun.*, vol. 28, no. 5, pp. 8–8, Oct. 2021.

[2] W. Tong and P. Zhu, *6G: The Next Horizon*. Cambridge: Cambridge University Press, 2021.

[3] C.-X. Wang, X. You, X. Gao, X. Zhu, Z. Li, C. Zhang, H. Wang, Y. Huang, Y. Chen, H. Haas *et al.*, "On the road to 6G: Visions, requirements, key technologies and testbeds," *IEEE Commun. Surveys Tuts.*, vol. 25, no. 2, pp. 905–974, 2nd Quart. 2023.

[4] M. Al-Quraan, L. Mohjazi, L. Bariah, A. Centeno, A. Zoha, K. Arshad, K. Assaleh, S. Muhaidat, M. Debbah, and M. A. Imran, "Edge-native intelligence for 6G communications driven by federated learning: A survey of trends and challenges," *IEEE Trans. Emerg. Topics Comput. Intell.*, vol. 7, no. 3, pp. 957–979, Jan. 2023.

[5] J. Wu, R. Li, X. An, C. Peng, Z. Liu, J. Crowcroft, and H. Zhang, "Toward native artificial intelligence in 6G networks: System design, architectures, and paradigms," *arXiv preprint arXiv:2103.02823*, 2021.

[6] P. Yang, Y. Xiao, M. Xiao, and S. Li, "6G wireless communications: Vision and potential techniques," *IEEE Netw.*, vol. 33, no. 4, pp. 70–75, Jul.-Aug. 2019.

[7] S. Dang, O. Amin, B. Shihada, and M.-S. Alouini, "What should 6G be?" *Nat. Electron.*, vol. 3, no. 1, pp. 20–29, Jan. 2020.

[8] F. Liu, Y. Cui, C. Masouros, J. Xu, T. X. Han, Y. C. Eldar, and S. Buzzi, "Integrated sensing and communications: Toward dual-functional wireless networks for 6G and beyond," *IEEE J. Sel. Areas Commun.*, vol. 40, no. 6, pp. 1728–1767, Jun. 2022.

[9] D. K. P. Tan, J. He, Y. Li, A. Bayesteh, Y. Chen, P. Zhu, and W. Tong, "Integrated sensing and communication in 6G: Motivations, use cases, requirements, challenges and future directions," in *Proc. IEEE JC&S*, Feb. 2021, pp. 1–6.

[10] D. Wen, P. Liu, G. Zhu, Y. Shi, J. Xu, Y. C. Eldar, and S. Cui, "Task-oriented sensing, computation, and communication integration for multi-device edge AI," *IEEE Trans. Wireless Commun.*, vol. 23, no. 3, pp. 2486–2502, Mar. 2024.

[11] X. Wang, X. Wang, and S. Mao, "RF sensing in the internet of things: A general deep learning framework," *IEEE Commun. Mag.*, vol. 56, no. 9, pp. 62–67, Sep. 2018.

[12] Y. Ma, G. Zhou, and S. Wang, "WiFi sensing with channel state information: A survey," *ACM Comput. Surv.*, vol. 52, no. 3, pp. 1–36, Jun. 2019.

[13] J. Hu, Z. Chen, T. Zheng, R. Schober, and J. Luo, "HoloFed: Environment-adaptive positioning via multi-band reconfigurable holographic surfaces and federated learning," *IEEE J. Sel. Areas Commun.*, vol. 41, no. 12, pp. 3736–3751, Dec. 2023.

[14] J. Hu, D. Niyato, and J. Luo, "Cross-domain learning framework for tracking users in RIS-aided multi-band ISAC systems with sparse labeled data," *IEEE J. Sel. Areas Commun.*, 2024, early access, doi: 10.1109/JSAC.2024.3414600.

[15] G. Li, S. Wang, J. Li, R. Wang, F. Liu, M. Zhang, X. Peng, and T. X. Han, "Rethinking the tradeoff in integrated sensing and communication: Recognition accuracy versus communication rate," *arXiv preprint arXiv:2107.09621*, 2021.

[16] Y. He, G. Yu, Y. Cai, and H. Luo, "Integrated sensing, computation, and communication: System framework and performance optimization," *IEEE Trans. Wireless Commun.*, vol. 23, no. 2, pp. 1114–1128, Feb. 2024.

[17] C. Shi, F. Wang, S. Salous, and J. Zhou, "Joint subcarrier assignment and power allocation strategy for integrated radar and communications system based on power minimization," *IEEE Sensors J.*, vol. 19, no. 23, pp. 11 167–11 179, Dec. 2019.

[18] C. Shi, F. Wang, M. Sellathurai, J. Zhou, and S. Salous, "Power minimization-based robust OFDM radar waveform design for radar and communication systems in coexistence," *IEEE Trans. Signal Process.*, vol. 66, no. 5, pp. 1316–1330, Mar. 2017.

[19] J. A. Mahal, A. Khawar, A. Abdelhadi, and T. C. Clancy, "Spectral coexistence of MIMO radar and MIMO cellular system," *IEEE Trans. Aerosp. Electron. Syst.*, vol. 53, no. 2, pp. 655–668, Apr. 2017.

[20] Y. He, J. Liu, M. Li, G. Yu, J. Han, and K. Ren, "SenCom: Integrated sensing and communication with practical WiFi," in *Proc. 29th ACM MobiCom*, Oct. 2023, pp. 1–16.

[21] J. Hu, T. Zheng, Z. Chen, H. Wang, and J. Luo, "MUSE-Fi: Contactless muti-person sensing exploiting near-field Wi-Fi channel variation," in *Proc. 29th ACM MobiCom*, Oct. 2023, pp. 1–15.

[22] W. Chen, K. Niu, D. Zhao, R. Zheng, D. Wu, W. Wang, L. Wang, and D. Zhang, "Robust dynamic hand gesture interaction using LTE terminals," in *Proc. ACM/IEEE IPSN*, 2020, pp. 109–120.

[23] S. M. Hernandez and E. Bulut, "WiFi sensing on the edge: Signal processing techniques and challenges for real-world systems," *IEEE Commun. Surveys Tuts.*, vol. 25, no. 1, pp. 46–76, 1st Quart. 2022.

[24] E. Perahia and R. Stacey, *Next Generation Wireless LANs: 802.11n and 802.11ac*. Cambridge University Press, 2013.

[25] A. Hassanien, M. G. Amin, Y. D. Zhang, and B. Himed, "A dual-function MIMO radar-communications system using PSK modulation," in *Proc. 24th EUSIPCO*, Aug. 2016, pp. 1613–1617.

[26] G. N. Saddik, R. S. Singh, and E. R. Brown, "Ultra-wideband multifunctional communications/radar system," *IEEE Trans. Microw. Theory Tech.*, vol. 55, no. 7, pp. 1431–1437, Jul. 2007.

[27] M. Roberton and E. Brown, "Integrated radar and communications based on chirped spread-spectrum techniques," in *Proc. IEEE MTT-S IMS*, Jun. 2003, pp. 611–614.

[28] M. Nowak, M. Wicks, Z. Zhang, and Z. Wu, "Co-designed radar-communication using linear frequency modulation waveform," *IEEE Aerosp. Electron. Syst. Mag.*, vol. 31, no. 10, pp. 28–35, Oct. 2016.

[29] R. Xie, K. Luo, and T. Jiang, "Waveform design for LFM-MPSK-based integrated radar and communication toward IoT applications," *IEEE Internet Things J.*, vol. 9, no. 7, pp. 5128–5141, Apr. 2021.

[30] T. Huang, N. Shlezinger, X. Xu, Y. Liu, and Y. C. Eldar, "MAJoRCom: A dual-function radar communication system using index modulation," *IEEE Trans. Signal Process.*, vol. 68, pp. 3423–3438, May 2020.

[31] D. Ma, N. Shlezinger, T. Huang, Y. Liu, and Y. C. Eldar, "FRaC: FMCW-based joint radar-communications system via index modulation," *IEEE J. Sel. Topics Signal Process.*, vol. 15, no. 6, pp. 1348–1364, Nov. 2021.

[32] R. Zhang, B. Shim, W. Yuan, M. Di Renzo, X. Dang, and W. Wu, "Integrated sensing and communication waveform design with sparse vector coding: Low sidelobes and ultra reliability," *IEEE Trans. Veh. Technol.*, vol. 71, no. 4, pp. 4489–4494, Apr. 2022.

[33] K. Wu, J. A. Zhang, Z. Ni, X. Huang, Y. J. Guo, and S. Chen, "Joint communications and sensing employing optimized MIMO-OFDM signals," *IEEE Internet Things J.*, 2023.

[34] F. Liu, L. Zhou, C. Masouros, A. Li, W. Luo, and A. Petropulu, "Toward dual-functional radar-communication systems: Optimal waveform design," *IEEE Signal Process.*, vol. 66, no. 16, pp. 4264–4279, Aug. 2018.

[35] Q. Feng, J. Pang, M. Maso, M. Debbah, and W. Tong, "IDFT-VFDM for supplementary uplink and LTE-NR co-existence," *IEEE Trans. Wireless Commun.*, vol. 19, no. 5, pp. 3435–3448, May 2020.

[36] L. S. Cardoso, M. Kobayashi, F. R. P. Cavalcanti, and M. Debbah, "Vandermonde-subspace frequency division multiplexing for two-tiered cognitive radio networks," *IEEE Trans. Commun.*, vol. 61, no. 6, pp. 2212–2220, Jun. 2013.

[37] M. Maso, L. S. Cardoso, M. Debbah, and L. Vangelista, "Channel estimation impact for LTE small cells based on MU-VFDM," in *Proc. IEEE WCNC*, Apr. 2012, pp. 2560–2565.

[38] C. Sturm and W. Wiesbeck, "Waveform design and signal processing aspects for fusion of wireless communications and radar sensing," *Proc. IEEE*, vol. 99, no. 7, pp. 1236–1259, Jul. 2011.

[39] Y. He, Y. Cai, H. Mao, and G. Yu, "RIS-assisted communication radar coexistence: Joint beamforming design and analysis," *IEEE J. Sel. Areas Commun.*, vol. 40, no. 7, pp. 2131–2145, Jul. 2022.

[40] M. A. Richards, J. Scheer, W. A. Holm, and W. L. Melvin, "Principles of Modern Radar," 2010.

[41] P. Stoica, H. He, and J. Li, "New algorithms for designing unimodular sequences with good correlation properties," *IEEE Trans. Signal Process.*, vol. 57, no. 4, pp. 1415–1425, Apr. 2009.

[42] Y. Sun, P. Babu, and D. P. Palomar, "Majorization-minimization algorithms in signal processing, communications, and machine learning," *IEEE Trans. Signal Process.*, vol. 65, no. 3, pp. 794–816, Feb. 2016.

[43] M. Razaviyayn, M. Hong, and Z.-Q. Luo, "A unified convergence analysis of block successive minimization methods for nonsmooth optimization," *SIAM J. Optimization*, vol. 23, no. 2, pp. 1126–1153, 2013.

[44] J. Song, P. Babu, and D. P. Palomar, "Optimization methods for designing sequences with low autocorrelation sidelobes," *IEEE Trans. Signal Process.*, vol. 63, no. 15, pp. 3998–4009, Aug. 2015.

[45] R. A. Horn and C. R. Johnson, *Matrix Analysis*. Cambridge university press, 2012.

[46] L.-S. Tsai and Y. T. Su, "Transform domain approach for sequence design and its applications," *IEEE J. Sel. Areas Commun.*, vol. 24, no. 1, pp. 75–83, Jan. 2005.

[47] L. Zhao, J. Song, P. Babu, and D. P. Palomar, "A unified framework for low autocorrelation sequence design via majorization–minimization," *IEEE Trans. Signal Process.*, vol. 65, no. 2, pp. 438–453, Jan. 2016.

[48] W. Liu, Q. Feng, J. Pang, Q. Hu, R. Yin, and G. Yu, "Robust rate-maximization rrecoder design for VFDM system," *IEEE Trans Veh. Technol.*, vol. 69, no. 3, pp. 2747–2757, Mar. 2020.